

elastically will be more important than their elastic counterparts. In this region, Eqs. (5) give a simple approximation to the Drell-Walecka form factors. The somewhat unphysical appearance of the factor $(1-x^2)$ is due to the overly crude nuclear model adopted in the derivation of Eq. (3a); for the same reason, the $(1-x^2)$ is unreliable for $x \approx 1$. It is tempting to replace $(1-x^2)$ by $\exp(-x^2)$, which certainly looks more plausible, but the resulting equation will again be unreliable for large x . In fact, a good criterion for the region of validity of

the approximate Eqs. (5) is the requirement that $(1-x^2) \approx \exp(-x^2)$. It is also essential that $|\mathbf{q}| \gtrsim 2P_f$, since otherwise both the shape and the nonzero region of the form factors are affected.³

ACKNOWLEDGMENTS

It is a pleasure to thank Gary Feldman for pointing out the interest of this problem, and Professor R. J. Glauber for a very helpful discussion.

Inelastic Alpha Scattering and Associated Gamma Radiation. III

DAVID R. INGLIS

Argonne National Laboratory, Argonne, Illinois*

(Received 9 December 1966)

In a 0-2-0 transition in a deformed nucleus excited by inelastic scattering of α particles, the pattern of γ radiation sometimes rotates rapidly backward as the α -particle scattering angle is increased. Previous papers employing a two-dimensional model have shown that this striking behavior may be attributed to the "beats" between incoming and outgoing waves at the edges of the nucleus. The most conspicuous effect there neglected was that of the "focus" of intensity of each of the distorted waves in the middle of its "shadow side" of the nucleus. Here it is shown that the influence of this effect modifies but need not destroy the reverse-rotation phenomenon, and that it provides an explanation for the failure of the reverse rotation to persist for small-angle scattering in most of the observations.

INTRODUCTION

THE main purpose of the previous papers¹ was to show that a striking phenomenon,²⁻⁴ otherwise reproduced theoretically^{2,5} only via less transparent computations, can be qualitatively understood in terms of a model treated with rather simple algebra. This is thought to give a better physical appreciation of inelastic scattering in general and of this phenomenon in particular. Such clarification is useful only so long as it remains simple. The temptation should be resisted to push it too far. Nevertheless, it is perhaps desirable to investigate the effect of contributions that have heretofore been neglected with somewhat questionable justification. The fit to experimental data leaves something to be desired, both in respect to understanding why the reverse rotation usually seems to cease near forward α

scattering and why the phenomenon varies so rapidly with bombarding energy.

While the previous treatments of the two-dimensional model have been based explicitly on the assumption of an almost-black nucleus, this assumption is not essential. The emphasis on the edge of the nucleus as the region where the phases are important can be provided just as effectively by the surface-interaction approximation which was used and seems natural for a deformed nucleus. The amplitude of waves inside is simply not coupled to the deformation. The assumption of constant wavelength around the relevant edges is essential to the simplified treatment, but it is as apt to be satisfied for a rather transparent nucleus as for a nearly opaque one.

The importance of a focus of the incoming wave at the far side of the nucleus has been emphasized by McCarthy,⁶ Austern,⁷ and others. It gives rise to backward contributions to scattering and direct reactions in a manner analogous to the "cat's eye" optics of the little glass spheres in highway reflectors. In the amplitude function of Fig. 4 of paper II (taken from Fig. 5 of Ref. 7), the trend was approximated by linear functions but for simplicity the high peak⁸ of amplitude at the

* Work performed under the auspices of the U. S. Atomic Energy Commission.

¹ D. R. Inglis, Phys. Letters **10**, 336 (1964); *Preludes in Theoretical Physics in Honor of V. F. Weisskopf*, edited by A. de-Shalit, H. Feshbach, and L. van Hove (North-Holland Publishing Company, Amsterdam, 1966) (cited as I); Phys. Rev. **142**, 591 (1966) (cited as II). See also B. J. Verhaar and L. D. Tolsma, Phys. Letters **17**, 53 (1965).

² D. K. McDaniels, D. L. Hendrie, R. H. Bassel, and G. R. Satchler, Phys. Letters **1**, 295 (1962).

³ W. W. Eidson, J. G. Cramer, Jr., D. E. Blatchely, and R. D. Bent, Nucl. Phys. **55**, 613 (1964).

⁴ D. E. Blatchely and R. D. Bent, Nucl. Phys. **61**, 641 (1965).

⁵ E. V. Inopin and S. Shehata, Nucl. Phys. **50**, 317 (1964); J. G. Cramer, Jr. and W. W. Eidson, *ibid.* **55**, 593 (1964).

⁶ I. E. McCarthy, Nucl. Phys. **11**, 571 (1959).

⁷ N. Austern, Ann. Phys. (N. Y.) **15**, 299 (1961).

⁸ The peak in Fig. 5 of Ref. 7 is based on the nearly-black-nucleus approximation and represents the meeting of waves coming around the surface from various azimuths. The focus may be quite as pronounced when waves come partially through the body of the nucleus, as McCarthy has illustrated in Ref. 6.

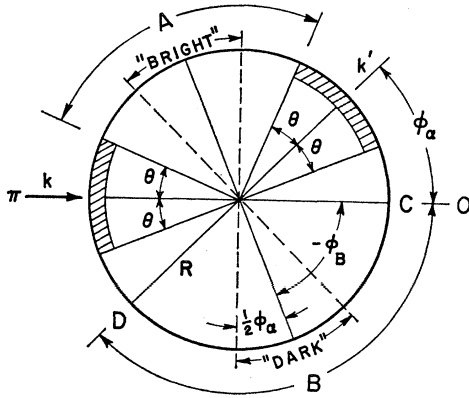


FIG. 1. Angles used in the two-dimensional model and the regions of the nuclear surface that contribute terms to the matrix elements.

focus was ignored in paper II. The next logical departure from complete simplicity of the treatment is thus to take this peak into account, in both the incoming and outgoing distorted waves.

MATRIX ELEMENTS AS MODIFIED BY THE FOCAL SPOTS

The matrix elements giving rise to the nuclear excitation consist of contributions from regions *A* and *B* (the neighborhoods of the "bright" and "dark" sectors) indicated in Fig. 1, as treated in papers I and II, and in addition the contributions from the "focal" points *C* and *D* on the far side of the nucleus for the incoming and outgoing wave, respectively. That is,

$$\langle m | \mathcal{H}' | i \rangle = \langle m | \mathcal{H}' | i \rangle_A + \langle m | \mathcal{H}' | i \rangle_B + \langle m | \mathcal{H}' | i \rangle_{C+D}. \quad (1)$$

The first two terms, the contributions from regions *A* and *B*, may be taken to be as specified by Eq. (5) of II. We shall compare three cases, case 1 being that treated in earlier papers with $\langle m | \mathcal{H}' | i \rangle_{C+D} = 0$. Otherwise, the contributions from *C* and *D* are each assumed to contain a δ function (multiplied by an amplitude *Y*) to represent the "spike" of amplitude at the focus, and to contain the overlap of the incoming and outgoing waves (with appropriate phase) and the angle function of the nuclear rotation.

Case 2 is based on the simple assumption that the wavelengths are constant all around the edge of the nucleus, so that the contribution from *C* and *D* may be written

$$\begin{aligned} \langle m | \mathcal{H}' | i \rangle_{C+D} &= Y \{ e^{i[kR\pi/2 + k'R(\phi_\alpha - \pi/2)]} \\ &\quad + e^{im(\pi - \phi_\alpha)} e^{i[kR(\phi_\alpha - \pi/2) + k'R\pi/2]} \} \\ &= 2Y e^{i\frac{1}{2}[m(\pi - \phi_\alpha) + \gamma]} \cos\left[\frac{1}{2}(D - m)(\pi - \phi_\alpha)\right], \end{aligned} \quad (2)$$

with $\gamma = S\phi_\alpha$, $S = (k + k')R$, $D = (k - k')R$, $R =$ undistorted radius. The amplitude factor *Y* of the spikes is real and is discussed further below.

Actually, one does not expect the wavelength to be constant clear around the nucleus. The most important deviation from this constancy is in the region near the point where the approximately plane waves first touch the surface tangentially. In case 3, the very slow variation of phase on the surface in this region is approximated by assuming that the phase is constant within a zone defined by a cone of half-angle θ centered on the axis of incidence and within a similar zone in the outgoing wave. On the basis of Fig. 4 of II as an example, it was assumed in II that $\theta = \frac{1}{8}\pi$ or slightly larger. For scattering angles smaller than θ we then have

$$\begin{aligned} \langle m | \mathcal{H}' | i \rangle_{C+D} &= Y \{ e^{i[kR\pi/2 + k'R(\theta - \pi/2)]} \\ &\quad + e^{im(\pi - \phi_\alpha)} e^{i[kR(\theta - \pi/2) + k'R\pi/2]} \} \\ &= 2Y e^{i\frac{1}{2}[m(\pi - \phi_\alpha) + S\theta]} \cos\eta_m, \end{aligned} \quad (3)$$

with

$$\begin{aligned} \eta_m &= \frac{1}{2}[D(\pi - \theta) - m(\pi - \phi_\alpha)] \\ &= \frac{1}{2}(D - m)(\pi - \phi_\alpha) + \frac{1}{2}D(\phi_\alpha - \theta). \end{aligned}$$

Here $\frac{1}{2}\pi - \theta$ enters as the angular displacement over which the phase varies, measured from the equatorial plane of each wave (where the phase factor is set equal to unity).

The magnitude of *Y*, the amplitude to be associated with the spikes at the two foci, must be examined in the light of the fact that the two-dimensional treatment is a model of a three-dimensional nucleus. A spike is narrow not only in the equatorial dimension measured by ϕ , but also in the latitude dimension normal to that. The sharpness and amplitude of the focal spot may of course depend on the details of the optical model used, but we may make a rough estimate of a reasonable magnitude by again taking the spike in Fig. 4 of II, taken from Austern's paper,⁷ as an example. The amplitude drops by a factor $1/e$ in about 0.2 rad and hence the $1/e$ radius of the focal spot is $\rho_0 = 0.2R$. Its peak height above the smoothed background is $A_s = 1.5$ on the scale on which the amplitude is unity at the maximum on the incident side. The surface integral of a radial Gaussian of these dimensions is the peak height multiplied by the area of the circle of this radius; i.e.,

$$\int_0^\infty \exp[-(\rho/\rho_0)^2] \rho d\rho = \pi\rho_0^2.$$

In the calculation of the competing terms of the matrix element, a one dimensional integral around the equator is used to represent a two dimensional integral over an equatorial band. The determination of the effective width of the band is suggested in Fig. 2, which should be studied in conjunction with Fig. 5 of II. The optical path difference between a scattering at the equator and one at the edge of the band is $2\Delta \sin\frac{1}{2}\phi_\alpha$, where Δ is the difference of radii indicated at the top of Fig. 2, and the criterion for coherence between contributions from

different latitudes within the band is

$$2\Delta \sin \frac{1}{2}\phi_\alpha \lesssim \frac{1}{4}\lambda.$$

With $\lambda \approx R$ and $\phi_\alpha \approx \frac{1}{2}\pi$, one has $\Delta \approx R/6$ and the angular half-width of the band is $\zeta = \cos^{-1}(1 - \Delta/R) \approx 0.6$ rad. For smaller ϕ_α this ζ becomes larger, up to the limit $\frac{1}{2}\pi$. Thus the band is about 1 rad wide and the element of integration $d\phi$ (rad) in the one-dimensional integral represents a solid angle of the order of $d\phi$ (rad²) in the two dimensional integral. On the same scale, the contribution of the spike at C is then $Y = \pi(\rho_0/R)^2 A_s A_f = \pi(0.2)^2(1.5)A_f \approx 0.2$ since A_f , the amplitude of the outgoing wave, remains fairly close to unity at the relevant angles. The contribution at D is the same with A_f replaced by A_i . Since the magnitude of the spike must depend on detailed assumptions about nuclear opacity and the like, it is reasonable to consider Y as an adjustable parameter with this as its order of magnitude.

ORIENTATION OF THE GAMMA PATTERN

The orientation angle ϕ_α of the radiation pattern may be determined as in II, with the algebra modified only slightly by the inclusion of additional terms. In the earlier discussion, as implied⁹ by Eqs. (5) and (12) of II, the result was

$$C_m e^{i\zeta m} = v_m + w_m e^{i\gamma} = (\beta/\pi)^{\frac{1}{2}} e^{i(\gamma/2 + m\phi_B)} \{ \langle m | \mathcal{J}C | i \rangle_A + \langle M | \mathcal{J}C | i \rangle_B \}, \quad (4)$$

with $\phi_B = \frac{1}{2}(\phi_\alpha - \pi)$. With the added term of Eq. (1), this is replaced by

$$C_m e^{i\delta m} = v_m + w_m e^{i\gamma} + (\beta/\pi)^{\frac{1}{2}} e^{i(\gamma/2 + m\phi_B)} \langle m | \mathcal{J}C | i \rangle_{C+D} \equiv \mathcal{R}_m + i \mathcal{I}_m. \quad (5)$$

With $L=2$, the case of immediate experimental interest, the orientation angle ϕ_0 of the gamma pattern is given by Eqs. (13) and (14) of II as

$$4(\phi_0 - \phi_B) = \delta_{-2} - \delta_2, \\ e^{i4(\phi_0 - \phi_B)} = (\mathcal{R}_2 - i \mathcal{I}_2)(\mathcal{R}_{-2} + i \mathcal{I}_{-2}) / C_2 C_{-2}, \quad (6)$$

$$\tan 4(\phi_0 - \phi_B) = (\mathcal{R}_2 \mathcal{I}_{-2} - \mathcal{R}_{-2} \mathcal{I}_2) / (\mathcal{R}_2 \mathcal{R}_{-2} + \mathcal{I}_2 \mathcal{I}_{-2}).$$

For case 2, with constant wavelength all the way around, and for case 3 in the region $\phi_\alpha > \theta$ in which the constant-wavelength sectors encounter the foci, Eqs. (2) and (5) yield

$$\mathcal{R}_m = v_m + (w_m + z_m) \cos \gamma, \quad \phi_\alpha > \theta \quad (7) \\ \mathcal{I}_m = (w_m + z_m) \sin \gamma,$$

with

$$z_m = 2(\beta/\pi)^{\frac{1}{2}} Y \cos[\frac{1}{2}(D - m)(\pi - \phi_\alpha)].$$

[The expressions for this z_m and η_m of Eq. (3) may be slightly simplified by putting $\frac{1}{2}(\phi_\alpha - \pi) = \phi_B$, but this could give a false impression of the origin of these terms which arise, in fact, from interference between the two foci.] For case 3 at small, scattering angles $\phi_\alpha < \theta$

⁹ In Eq. (5) of II, π/β is misprinted as π/B .

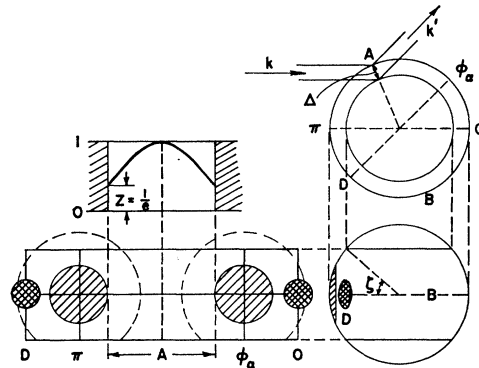


FIG. 2. Determination of the width of the equatorial band within which scattering at various latitudes is coherent. The upper sphere is viewed along the polar axis, the lower sphere from the equatorial plane. The strip to the left of the lower sphere is the equatorial band flattened out. The small dark circles represent the areas of the focal spots and the larger shaded circles are the "doldrum" regions in which the phase is assumed to remain constant in case 3.

Eqs. (3) and (5) lead instead to

$$\mathcal{R}_m = v_m + w_m \cos \gamma + u_m \cos \xi, \\ \mathcal{I}_m = w_m \sin \gamma + u_m \sin \xi, \quad \phi_\alpha < \theta \quad (8) \\ u_m = 2(\beta/\pi)^{1/2} Y \cos \eta_m, \\ \xi = \gamma + \frac{1}{2}S(\theta - \phi_\alpha) = \frac{1}{2}S(\phi_\alpha + \theta).$$

In the case of a uniform variation of phase around the circle (case 2) the result given in Eqs. (7) is remarkably simple: w_m of the earlier analysis with $Y=0$ is replaced by $w_m + z_m$. Thus Eqs. (16) and (17) of II also apply with the same slight modification and one again has the result in reasonably simple analytical form.

$$\phi_0 = \phi_B - \frac{1}{4} \tan^{-1} \left(\frac{q \sin \gamma}{p + \cos \gamma} \right), \\ p = S_0/S_+, \quad q = S_-/S_+, \quad (9) \\ S_0 = v_2 v_{-2} + (w_2 + z_2)(w_{-2} + z_{-2}), \\ S_\pm = v_{-2}(w_2 + z_2) \pm v_2(w_{-2} + z_{-2}).$$

The first of these equations is an important result discussed in I and II, in I with the approximation $q=1$ arising from neglect of the small contribution w_{-2} . In this approximation, a *physical appreciation* of the apparent struggle between oscillation and reverse rotation is obtained by considering the limiting cases of large and small p . For large p , $\tan^{-1}[(\sin \gamma)/p] \approx (\sin \gamma)/p$ and ϕ_0 executes a small-amplitude sinusoidal oscillation about the approximate recoil direction ϕ_B . For small p , one has $\tan^{-1}(\tan \gamma) = \gamma$ and ϕ_0 is linear in ϕ_α with a steep negative slope,

$$\phi_0 \approx \phi_B - \frac{1}{4}(k+k')R\phi_\alpha.$$

In intermediate situations one obtains as an intermediate result the characteristic S-shaped curves illustrated in detail in I and II.

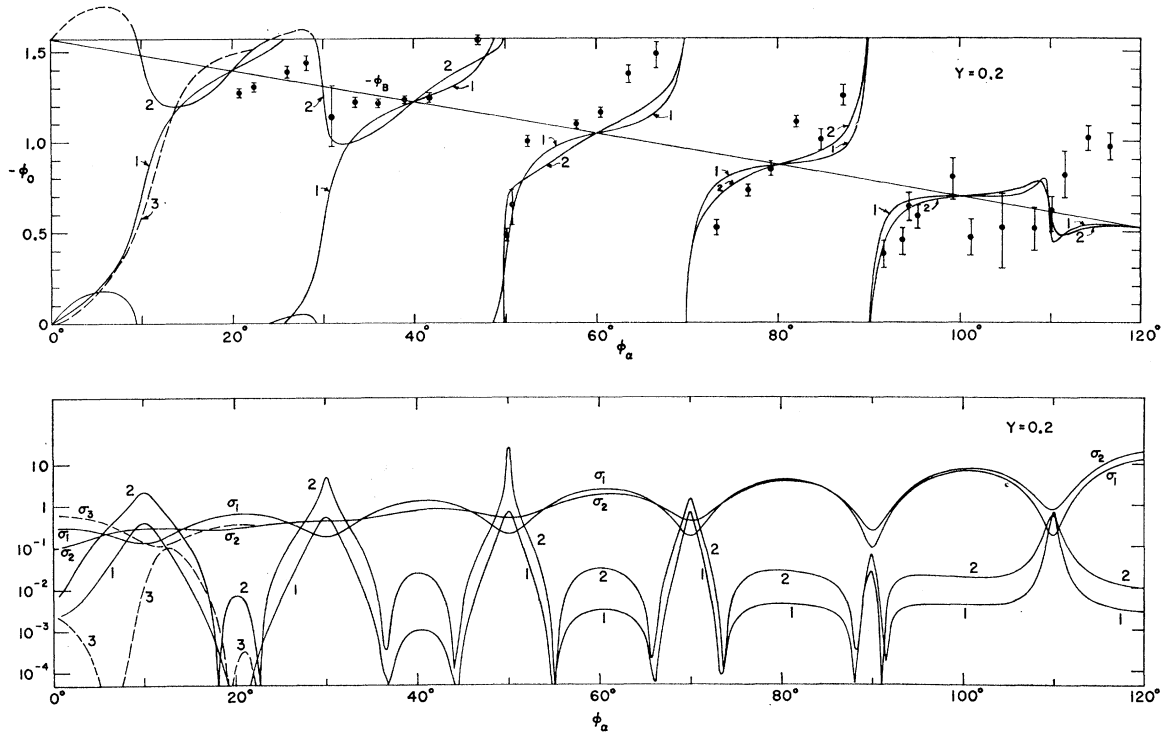


FIG. 3. *Upper panel:* The variation of ϕ_0 giving the orientation of the γ pattern as it varies with scattering angle. The numbers on the curves denote the three cases. Case 1: no contribution from the focal spots. Case 2: phase at the focal spots calculated with constant wavelength in each distorted wave around the edge of the nucleus. Case 3: each distorted wave given constant phase in the "doldrum" region within 22.5° of the point at which the wave is tangent to the nuclear surface. Curve 3 coincides with curve 2 for $\phi_\alpha > 22.5^\circ$ and is shown as a broken curve at smaller angles. The experimental points are for Mg^{24} at 22.5 MeV, from Ref. 3, the same as appear in Fig. 6 of II.

Lower panel: The differential inelastic cross section σ for the three cases and the ratio A/B denoted by 1, 2 and 3 for the three cases. A/B indicates the depth of the minimum between lobes of the rosette pattern. Note the logarithmic scale on which in most instances the scattering patterns, despite their flat appearance, have peak-to-valley ratios of the order of 10 while the minima of the rosette pattern are very deep.

The reverse rotation appears only when $p < 1$. With the focus terms taken into account, this criterion is simply modified by the presence of the z_m in the definition of p in Eq. (9). The simplicity of this modification arises from the fact that the quantity $\gamma = (k+k')R\phi_\alpha$ enters the calculation in two distinct but somewhat similar ways: (1) in determining the phase at the midpoints ϕ_A of the bright sector and $\phi_B = \frac{1}{2}(\phi_\alpha - \pi)$ of the shadow sector (from which the integrations determining the V_m and W_m are carried out in a symmetrical way), and (2) in determining the phase of the average (whence the factor $\frac{1}{2}$) contribution of the points C and D which are separated by $(\pi - \phi_\alpha)$. This latter phase is, of course, disturbed in case 3 in which the phase variation of each distorted wave is cut off at the angle θ , and the numerical evaluation is most conveniently carried out directly in the form of Eqs. (8). There it is seen that at most places ϕ_α is replaced by θ , but not where it is multiplied by m arising from the rotation factor of the wave function.

The action of the term in Y may be better appreciated by considering the case in which it alone is effective in orienting the nuclear excitation, that is, the case with

$Y \rightarrow \infty$ or with $v_m = w_m = 0$. In this case, from Eq. (3),

$$u_{exc} = \sum_m \langle m | \mathcal{H}C' | i \rangle_{C+D} e^{im\phi} \propto \sum e^{i\frac{1}{2}[m(\phi_\alpha) + S\theta]} \cos \eta_m e^{im\phi} = e^{i\frac{1}{2}S\theta} \sum \cos \eta_m e^{im\phi'}, \tag{10}$$

with $\phi' = \phi - \phi_B$ and $\phi_B = \frac{1}{2}(\phi_\alpha - \pi)$ as in II, so there is no phase difference between the two terms containing $e^{im\phi'}$. Hence $\phi'_0 = 0$ or $\phi_0 = \phi_B$. In other words, in Eq. (9), $S_\pm = 0$, $p = \infty$, and $\phi_0 = \phi_B - \frac{1}{4} \tan^{-1} 0 = \phi_B$. Equation (10) is written for the case involving θ ; but in the other case, with $\theta \rightarrow \phi_\alpha$, the result is clearly the same. The interactions at C and D thus freeze the four-petal rosette pattern of the γ rays in such a position that two opposite petals are equidistant from C and D , respectively, and there is no rapid rotation.

GRAPHICAL PRESENTATION OF THE INFLUENCE OF THE FOCUS

Numerical evaluation of Eqs. (6-9) for the gamma orientation angle ϕ_0 for case 2 and case 3 has been carried out for the focus-strength parameter $Y=0.2$ and 0.4. These are shown in the upper halves of Figs. 3

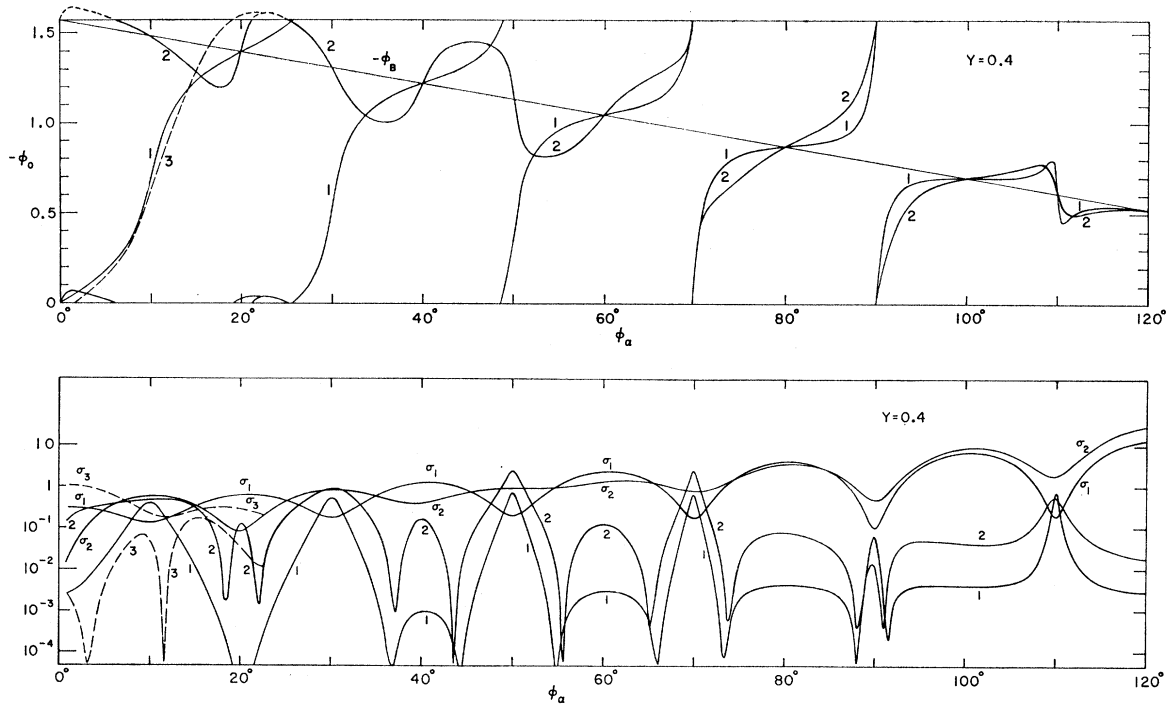


FIG. 4. Same as Fig. 3 except that the intensity of the foci of the distorted waves has been doubled by increasing the parameter Y from 0.2 to 0.4.

and 4 along with the curve for case 1, which refers to $Y=0$, for the sake of comparison. The other parameters used in these evaluations are the same as for Fig. 6 of II, including $Z=1/e$ and $W'=0.8$ which were chosen to fit the data in most of the angular range, particularly the cut-off of the reverse rotation beyond 100° . Curve 1 in Fig. 3 is thus the same as in Fig. 6 of II, though it looks different because the horizontal scale has been stretched. Case 2 and case 3 coincide for angles greater than $\theta=22.5^\circ$, and their common curve in this region is labeled simply "2."

The specific feature for which an explanation is sought in this paper is the failure of the reverse rotation to extend to fairly small-angle scattering ($\sim 15\text{--}40^\circ$) in many of the observations, as appears in Fig. 6 of II and in several of the graphs of Refs. 3 and 4. In this region, ϕ_0 instead seems to oscillate about the recoil direction ϕ_B . It is seen in Fig. 3 that the theoretical curve for case 2 with $Y=0.2$ (the estimated value) exhibits just such a behavior, and for case 3 the curve deviates from this general behavior (making an extra quarter revolution) only at angles below 15° , to which available observations do not extend. Since case 3 is based on the more consistent set of assumptions (it includes the effect of the doldrum region on both the lateral and focal contributions), it might be interesting to learn whether observations will reproduce this feature. Comparison of Fig. 4 with Fig. 3 indicates that the result is only moderately sensitive to the strength of the focal

spots. It shows that doubling Y further confines the region of reverse rotation to angles above 60° .

The inclusion of the focus effects thus improves the qualitative agreement with experiment in that it provides a reasonable explanation for the fact that the reverse rotation is observed predominantly in the region of $40\text{--}100^\circ$.

The diffraction pattern of the inelastic scattering, shown as the curves labeled σ in the lower panels of Figs. 3 and 4 rather consistently displays the feature that the maxima coincide with the points where the reverse-rotation curves of ϕ_0 cross the recoil direction ϕ_B , in agreement with the usual experimental result. These are the angles ϕ_α at which the maxima in the overlap between incident and final waves occur at the midpoints of the light and dark regions, near the line giving the recoil direction. This is where the excitation of the nucleus is strongest and fixes the maximum of the probability distribution of the long axis of the nuclear deformation, and thus the position ϕ_0 of the minimum of the γ pattern, in this direction.

The shape of the γ pattern [as given by Eq. (24) of II] is

$$\sigma(\phi_\gamma) = A + B \sin^2 2(\phi_\gamma - \phi_0). \quad (11)$$

Thus A is a measure of the depth of the minimum between the lobes of the rosette. The curves of A/B shown in Figs. 3 and 4 display considerably lower minima than are observed experimentally. It is perhaps

not surprising that the actual phenomenon is not as clean as the model in this respect. The observations of A/B (for example, Ref. 3, Fig. 10; Ref. 4, Fig. 7) show swings by a factor of about 20 between maxima and minima. The phase of the curves for A/B presents some difficulty and seems to be very sensitive to details not included in the theory. Both the two-dimensional model and the distorted-wave Born approximation (DWBA) show the principal maxima of A/B at the angles where the intensity is weakest (minima of σ , as though the intensity there is stolen from the petals of the rosette) and the curves in Figs. 3 and 4 also show much lower intermediate maxima. The experimental results for Mg^{24} tend to follow the broad intermediate maxima and to ignore the sharp maxima and for Si^{28} they show no clear trend.

ENERGY DEPENDENCE. RELATION BETWEEN "BEATS" AND A PARTIAL-WAVE ANALYSIS

This analysis has been presented in terms of distorted waves pictured as plane waves modified to bend around the surface in an appropriate manner, as indicated in Fig. 4 of I and Fig. 4 of II. Partial-wave analysis has been avoided for the sake of pictorial and analytic simplicity. The "beats" between incoming and outgoing waves may be seen most simply in this way. However, the beats, which determine the orientation of the nuclear excitation, must occur in the same way between the dominant partial waves of a partial-wave analysis of the distorted waves. The partial waves are characterized by their angular momentum, being determined by the circular symmetry of the unperturbed problem. At an energy at which the incident α grazing past the edge of the nucleus has integral angular momentum, the partial wave corresponding to this angular momentum would be expected to be dominant. The phase variation we have assumed around the edge of the nucleus is predominantly that of this partial wave. Thus the beats may be ascribed to partial waves as well as to the pictorial distorted waves we have discussed. In such terms as this, one can qualitatively understand the relatively recent discovery¹⁰ that the reverse rotation becomes alternatively active and quiescent as the incident energy is raised, in a manner presumably in consonance with the ascendancy of successive partial waves at the edge of the nucleus.

¹⁰ P. P. Singh, W. W. Eidson, *et al.* (private communication).

The simplest presumption would be that the incoming angular momentum $l_i \approx kR$ (with Coulomb deflection neglected) and the final angular momentum $l_f = k'R$ should differ by one unit so that each wave could correspond most closely to one partial wave. Quantitatively, this is not the case and the situation appears to be not quite so simple. In the example discussed on p. 596 of II, the case of Mg^{24} at 22.5 MeV, the numbers are $k = 5.03mc^2/e^2$, $k'/k = 0.964$ and the values of R (or r_0) suggested ranged from about $1.9\text{--}2.1 \times e^2/mc^2$, or roughly $2e^2/mc^2$. Thus $l_i = 10$ as the closest integer; but then $l_f = 9.64$, the difference $l_i - l_f$ being about $\frac{1}{3}$, rather than an integer. Thus it may be that the favorable situation is for k_i and k_f to be both fairly close to an integer such as 10, but for one to have more of 9 and the other more of 11 in its wave packet with comparable intensities. (Alternatively, both near a half integer might be favorable.) On change of energy, the next favorable situation would be anticipated with a change of k_i by about 10% (corresponding to a change of energy by about 20%) for such examples as this one.

CONCLUSION

Analysis of the nuclear rotational excitation and subsequent radiation in a two-dimensional model demonstrates that the reverse rotation of the γ -ray pattern can be legitimately understood as a result of the simple concept that backward-moving "beats" between incoming and outgoing waves occur at the lateral edges of the nucleus when the outgoing wave, of slightly longer wavelength, is moved "forward" with the increasing scattering angle. This simplified analysis alone leads to a reverse rotation beginning with very small scattering angles and extending out to some maximum angle such as 90° or beyond. For other than the very light nucleus C^{12} , the reverse rotation is observed predominantly in the region of $40\text{--}100^\circ$ and is lacking at smaller scattering angles. This cutoff at forward angles, too, may be obtained from the two-dimensional analysis by incorporating the next obvious step towards increasing complexity, namely, the effect of the large amplitude surface regions at the focal spots of the incoming and outgoing waves. This adaptability of the analysis adds credence to the simple "beat" concept as the basic source of the phenomenon.